Available online at www.sciencedirect.com
SCIENCE DIRECT®
International Journal of Heat and Mass Transfer 47 (2004) 1305–1312
International Journal of HEAT and MASS TRANSFER
www.elsevier.com/locate/ijhmt

Studies on high-temperature multilayer thermal insulations

Markus Spinnler [a,*], Edgar R.F. Winter [a,1], Raymond Viskanta [b,2]

[a] Lehrstuhl für Thermodynamik, Technische Universität München, D-85747 Garching, Germany
[b] School of Mechanical Engineering, Purdue University, West Lafayette, IN 47907, USA

Received 17 July 2003; received in revised form 18 August 2003

Abstract

Experimental and theoretical studies are reported on the determination of the effective thermal conductivities of multilayer thermal insulation systems with specially designed shields for application in high temperature fuel cells. An experimental apparatus and instrumentation have been designed and built to measure heat transfer through such insulation systems at temperatures up to 1000 °C. The insulations consisted of both fibrous and microporous materials. A theoretical model based on combined conduction and radiation heat transfer through porous materials capable of absorbing, emitting and scattering has been used to predict the temperature distribution and heat transfer in insulations comprised of the materials separated by multiple screens (shields). The experimental results obtained for several multilayer thermal insulation systems are reported, and the experimental data are compared with theoretical predictions to assess the effectiveness of the screens in reducing the effective thermal conductivity of the insulations.

Keywords: Effective thermal conductivity; Multilayer insulations; High temperature; Fuel cells

1. Introduction

Thermal insulations have been the subject of great interest and importance to thermal engineers and to the early development of heat transfer technologies [1,2]. During the last several decades developments in heat transfer and use of thermal insulations in emerging technologies have extended the range of applications from cryogenic temperatures to high temperatures under reentry conditions into planetary atmospheres. This paper is concerned with multilayer thermal insulations (MTIs) for high-temperature fuel cell applications.

MTIs have originally been developed for cryogenic applications for storing liquids and gases at very low temperatures. An account describing the early developments of thermal insulations including MTIs for cryogenic applications is available [3]. In order to understand the advantages of MTI in both low and high temperature applications, basic heat transfer mechanisms in porous media, namely radiation, gas and solid conduction have to be considered, whereas convection can be neglected. Thermal protection systems of cryogenic tanks generally use double-walls and evacuate the gap between the walls. This reduces both gas conduction and convection. Radiation heat transfer is reduced by means of highly reflective screens which are separated by polymeric or ceramic spacers for the sake of reducing solid conduction in these superinsulations [3]. For high-temperature reentry applications into the earth atmosphere the insulations are of different design [4,5]. At temperatures above 300 °C radiation becomes the dominant mode of heat transfer and this makes radiation screens suitable for high temperature applications at ambient pressure. The screens are positioned in a sandwich with optically dense spacer materials. Large research efforts have been undertaken to develop MTIs for space applications, especially heat shields for reentry vehicles [4,5] as well as in the use for high temperature (MCFC and SOFC) fuel cells [6,7].

Fuel cells are electrochemical devices that convert chemical energy of a fuel directly to electrical and

* Corresponding author. Fax: +49-89-289-162-18.
E-mail addresses: spinnler@td.mw.tum.de (M. Spinnler), viskanta@ecn.purdue.edu (R. Viskanta).
[1] Deceased.
[2] Tel.: +765-494-5632; fax: +765-494-0539.

0017-9310/$ - see front matter © 2003 Elsevier Ltd. All rights reserved.
doi:10.1016/j.ijheatmasstransfer.2003.08.012

Nomenclature

I	intensity of radiation
I_b	blackbody intensity of radiation integrated over the spectrum
k_{eff}	effective total thermal conductivity of a porous medium
$\tilde{k}_c$	effective conductivity for gas and solid conduction in a porous medium
L	thickness of insulation layer
$\tilde{n}$	effective index of refraction of porous medium
p	scattering phase function
q	total (conductive plus radiative) heat flux
q_R	radiative heat flux, see Eq. (2)
q_R^*	normalized radiative heat flux, q_R/q
T	temperature
T_R	radiation temperature, $\sqrt[3]{(T_1^2+T_2^2)(T_1+T_2)/4}$
T^*	normalized temperature, T/T_1
x	coordinate

Greek symbols

β	extinction coefficient
β_s	effective extinction coefficient with screens
β^*	normalized effective extinction coefficient, β/β_s
ε	emissivity
κ	absorption coefficient
ρ	reflectivity
ρ_β	scaled reflectance, defined by Eq. (5)
θ	polar angle
σ	scattering coefficient or Stefan–Boltzmann constant
τ	optical depth, $\tau = \beta x$
τ_L	optical thickness, $\tau_L = \beta L$
$\tau_{L,\beta}$	scaled optical thickness, see Eq. (5)
ϕ	porosity
ω	single scattering albedo
Ω	solid angle

Subscripts

1	refers to hot boundary
2	refers to cold boundary

thermal energy. They represent an ambitious emerging technology which has a promise not only to be efficient but which would simultaneously help industrial nations around the world to meet desired CO_2 reduction goals. A crucial issue in bringing fuel cell technology to maturity in the future is the need to develop very efficient thermal insulation systems. Effective insulation systems are highly desirable for ensuring a uniform fuel cell stack temperature which also promises the possibility of realizing electric load cycles at constant stack temperatures. Furthermore, highly efficient thermal protection systems are important for an optimal use of waste heat in order to reach maximum conversion efficiency.

Fig. 1 shows spacer materials for high temperature MTIs. The materials considered can be subdivided into three groups: fibers, microporous materials, and refractories (or fire clays). Fibrous materials combine a low density of about 100 $kg\,m^{-3}$ with a moderate thermal conductivity of 0.10 $W\,m^{-1}\,K^{-1}$ (20 °C) to 0.35 $W\,m^{-1}\,K^{-1}$ (1000 °C), respectively. Microporous materials available are of moderate density of less then 300 $kg\,m^{-3}$ together with a low thermal conductivity of 0.02 $W\,m^{-1}\,K^{-1}$ (20 °C) to 0.04 $W\,m^{-1}\,K^{-1}$ (1000 °C), respectively, whereas fire clays are both of high density (more than 300 $kg\,m^{-3}$) and have high thermal conductivity of up to 0.5 $W\,m^{-1}\,K^{-1}$ at 1000 °C.

Note that the very low thermal conductivity of microporous materials is due to their microporous structure with pore diameters below 0.1 μm. This is responsible for the reduction of the gaseous convection

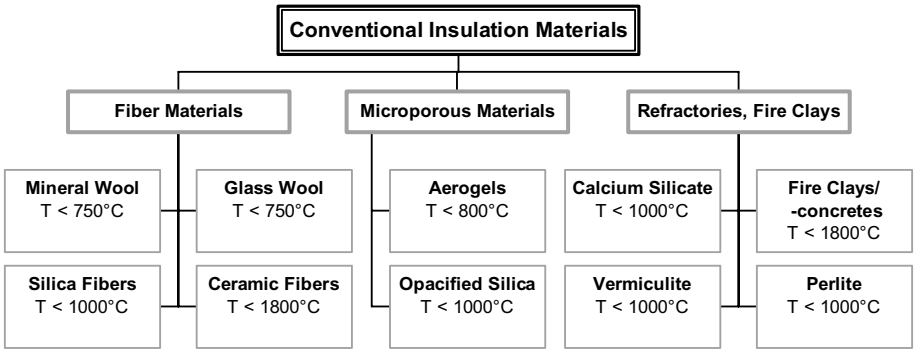

Fig. 1. Spacer materials suitable for MTI.

and conduction contributions to total heat transfer but with a somewhat higher fraction of solid conduction. Radiation is reduced by addition of, so called, infrared opacifiers of about 30% by weight. As refractories and fire clays are designed for mechanical strength and not for low thermal conductivity they will not be considered for use as spacer materials in this study.

The paper reports on an experimental and theoretical study of multilayer thermal insulations for high temperature fuel cell applications such as molten carbonate fuel cells (MCFC) and solid oxide fuel cells (SOFC). Experimental results are reported for insulations based on fibrous and microporous materials with and without multiple spacers. The effects of screens (shields) are investigated by using relatively low (stainless steel), intermediate (ceramic) and high (gold) reflectivity screens. Theoretical predictions based on a combined conduction radiation heat transfer model are compared with experimental data for the purpose of gaining improved understanding of complex heat transfer phenomena in MTIs.

2. Theoretical analysis

2.1. Analytical model

In a theoretical analysis of heat transfer through layered porous media gas and solid conduction as well as radiation need to be considered, and recent accounts are available [8,9]. As already mentioned, convective heat transfer in porous media of interest in this discussion is negligible [10,11]. A schematic diagram of a multilayer insulation is shown in Fig. 2. A low thermal conductivity filler is confined between two opaque boundaries. One or more thin screens are placed parallel to the boundaries to form a one-dimensional layer of MTI. The porous spacer material absorbs, emits and scatters thermal radiation. The screens are very thin but opaque and emit and reflect radiation diffusely. The steady-state heat transfer through the planar, one dimensional layer is assumed to be by combined conduction and radiation.

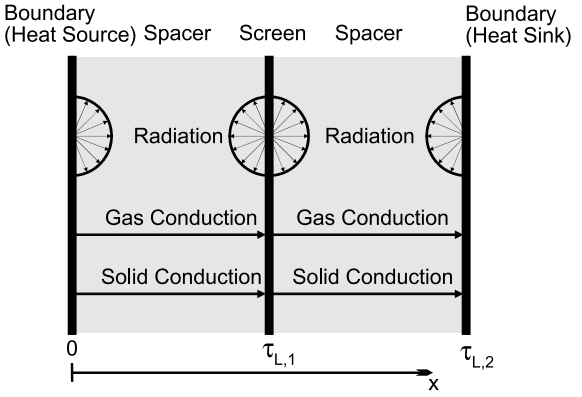

Fig. 2. Schematic diagram of a multilayer insulation with two spacer material layers and a single screen.

There are two possible ways for calculating the combined heat transfer in stacked systems with radiation screens [11]. For optically dense ($\tau_L \gg 1$) porous materials the effective thermal conductivity can be expressed in terms of the local radiation temperature T_R as

$$k_{\text{eff}} = \tilde{k}_c + \frac{16}{3}\frac{\tilde{n}^2}{\beta}\sigma T_R^3, \tag{1}$$

where $\tilde{k}_c$ is the effective thermal conductivity due to the gas and solid conduction. The second term in Eq. (1) represents "radiative conductivity" based on the Rosseland diffusion approximation. Plotting the conductivity as a function of T_R^3, its linear representation allows determination of gray Rosseland extinction coefficients β from the slope of the linear function. The effective thermal conductivity, $\tilde{k}_c$, which accounts for heat conduction in the gas and solid phases can be determined from the intercept of the ordinate at 0 K, which should be the same for samples with and without radiation screens.

We emphasize that the approximation, Eq. (1), is only valid for optically dense media having large opacities (i.e., $\tau_L > 15$) and fails to take proper account of radiation transfer in the vicinity of the screens. Preliminary calculations using the Rosseland diffusion approximation underestimated the effects of the screens [12].

The second approach is based on the conservation of energy equation in the layer, with the radiation contribution calculated using the radiative transfer equation. In this paper we adopt the latter approach for analyzing combined heat transfer.

Based on the physical model described, the governing steady-state energy equation is

$$\frac{dq}{dx} = \frac{d}{dx}\left[-\tilde{k}_c\frac{dT}{dx} + q_R(x)\right] = 0$$
$$\text{or} \quad -\tilde{k}_c\frac{dT}{dx} + q_R(x) = \text{constant}, \tag{2}$$

where the local radiative flux $q_R(x)$ is defined by

$$q_R(x) = \int_{\Omega=4\pi} I(x,\theta)\cos\theta\, d\Omega. \tag{3}$$

The intensity of radiation $I(x,\theta)$ is calculated from the radiative transfer equation (RTE) for an absorbing, emitting and scattering spacer material,

$$\cos\theta\frac{dI}{dx} = -\beta I + \kappa\tilde{n}^2 I_b(T) + \frac{\sigma}{2}\int_0^{\pi} I(x,\theta')\sin\theta'\, d\theta'. \tag{4}$$

The temperatures are imposed at the boundaries for the energy equation, Eq. (2), and for intensity at the boundaries and screens (shields) diffuse emission and reflection of radiation is considered at the surfaces.

Thermophysical and radiation characteristics of the spacer materials are needed as inputs before the model equations can be solved. These characteristics for porous media are described in some detail elsewhere [12] and will be only briefly discussed later.

The RTE cannot be solved analytically and further assumptions have to be made. The scaling model described by Lee and Buckius [13] is used. The scattering coefficient σ can be set to zero and scaled transmission and reflection coefficients are defined based on linear scattering for optically thin layers as documented elsewhere [13]. The optical thickness and reflectance can be scaled as

$$\tau_{L,\beta} = (1-\omega)\tau_L \quad \text{and} \quad \rho_\beta = 1 - \frac{2}{\frac{3}{4}\tau_L\omega + 2}. \tag{5}$$

Furthermore, the scaling model of Lee and Buckius [13] recommends splitting up the spacer material into a number N of optically thin, isothermal layers and thus separating radiation heat transfer into three subproblems, i.e., two irradiation problems from the hot side and cold side of each layer, respectively, as well as an emission problem with boundary temperatures generally set to zero. Discussions of heat transfer in gray radiatively participating media and steady-state heat transfer can be found in the literature [11,14]. The procedure suggested [13] yields so-called attenuation functions for transmittance, reflectance and emittance in each layer and q_R can be calculated by simply adding the three contributions. The details of the calculations are described elsewhere [12].

Fig. 3 shows a sketch of the multilayered system, consisting of k sections formed by the spacer and the two adjacent radiation screens. Each section again is subdivided in N isothermal, optically thin layers of $\Delta\tau_L$ thickness. As a temperature distribution is needed for calculating q_R, sectional temperature distribution has to be determined iteratively, and the heat flux through the system has to be varied numerically until a given cold side temperature of the system (T_2) is reached. The computational details are given elsewhere [12].

Comparison of the model predictions with published results given in literature [14,15] yielded good agreement in the case of strong scattering (i.e., high albedo) case, whereas some minor discrepancies were found for purely absorbing spacer materials [12].

3. Experimental studies

Effective thermal conductivity k_{eff} of MTIs were determined experimentally. The best means of obtaining thermal conductivity data in layered systems are through measurements using the guarded hot plate apparatus. A description of the general operating principles of the guarded hot plate apparatus can be found elsewhere [16].

Note that there are certain limitations in the general standards for measurements with the hot plate apparatus at higher temperatures. Normally, the hot plate is heated directly via electrical resistance which causes heater burnouts at hot plate temperatures above 800 °C. Furthermore, the thermal deformation of the (metallic) hot plate has to be avoided as an exact sample thickness is crucial for experimental accuracy. Fig. 4 shows a schematic diagram of the experimental set-up used for the measurements. Apart from the technical standards, an indirect system is used for heating a ceramic plate by means of a 24 kW infrared heater unit. With this setup,

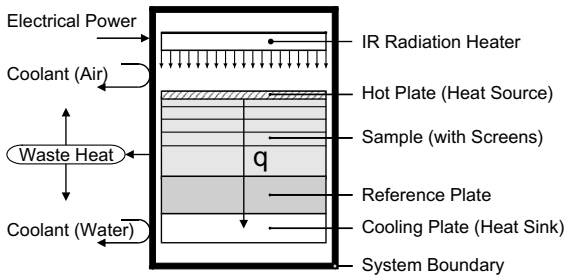

Fig. 4. Schematic diagram of the guarded hot plate apparatus.

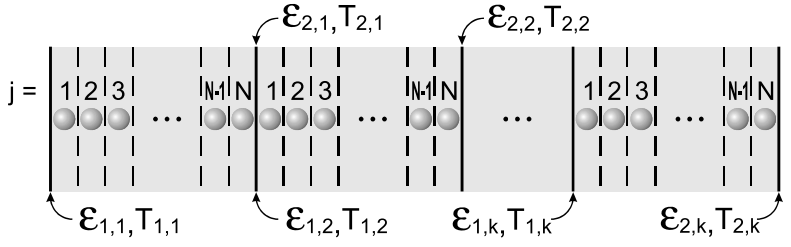

Fig. 3. Separation of the insulation system in k-sections and N-layers each.

hot plate temperatures of 1200 °C and higher can easily be achieved with no or very small deformation of the hot plate. As a reference, a PTFE plate with well established thermal conductivity of 0.139 $W m^{-1} K^{-1}$ is used together with a water cooled aluminum heat sink. Side insulations are applied according to the German standards [16], but no temperature guarding is used. Preliminary tests have shown negligible influence on the results by varying the sample thickness, justifying the assumption of negligible radial heat losses.

During the preliminary tests a horizontal set-up was used which employed an Inconel hot plate, but this arrangement resulted in certain limitations of the experimental accuracy due to thermal deformation. The main test series was carried out on a second (enhanced) apparatus in vertical orientation. A ceramic hot plate (SiC) showed no thermal deformation and an improved axial guideway for adjusting sample thickness with optimal accuracy was employed [12].

The experimental uncertainty for measuring the effective thermal conductivity was determined according to recommendations in [17, section F]. The maximum uncertainty was about 30% and the minimum was about 3%. The uncertainty depended on the temperature difference, the thickness and the thermal conductivity of the reference plate as well as on the temperature difference across the plate. Thickness of the test specimen was found to be crucial for measurement accuracy. The details are given elsewhere [12].

The physical characteristics of the commercially available spacer materials used in the tests are summarized in Table 1. A total of 14 (four without screens and 10 with screens) test MTIs were constructed and studied and each had four equally spaced shields made from either stainless steel (Cr 22 A15Y), gold or ceramic ($A1_2O_3$). The test MTIs were 30 mm in thickness. Detailed descriptions of specimen are provided in the dissertation [12]. In order to exclude disturbing influences of different spacer densities on the thermal conductivity, their weight and dimensions were controlled at the beginning and the end of each test series. The mechanical load pressure was generally adjusted to 10^5 Pa.

4. Results and discussion

4.1. Experimental results

According to the Rosseland diffusion approximation (see Section 2.1), the effective thermal conductivity k_{eff} is a function of the radiation temperature T_R to the third power. Fig. 5 illustrates representative results of measurements with the ordinate showing the effective thermal conductivities in [$W m^{-1} K^{-1}$] for samples with and without screens. The abscissa is the magnitude of radiation temperatures T_R^3 in [K^3]. In the experiments shown in Fig. 5, the silica fibers type "Isotherm 1000" by Frenzelit were used as spacer material with four (4) either stainless steel or gold screens at 5 mm apart, starting from the hot side. The emissivities of the screens

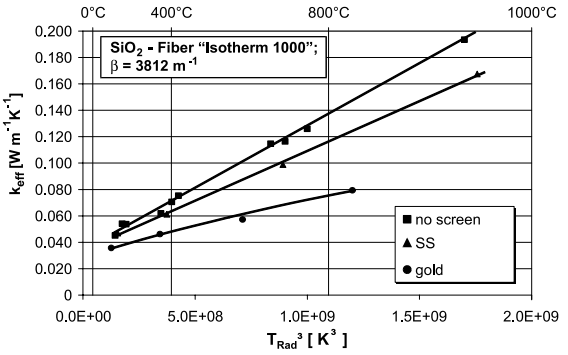

Fig. 5. Dependence of the effective thermal conductivity on T_R^3 for an insulation system: "Isotherm 1000" spacer material, four screens, total thickness of 30 mm.

Table 1
Summary of physical characteristics of spacer materials used in experiments

Material (manufacturer)	Chemical composition	Density (kg/m^3)	Porosity (%)	Avg. particle diameter (μm)
Isotherm 1000 (Frenzelit)[a]	≈95% SiO_2	140	94.9	6
HT 1000 (Klevers)[b]	≈4% Al_2O_3 ≈95% SiO_2	140	94.9	6
Saffil (ICI)[c]	≈96% Al_2O_3 ≈4% SiO_2	96	97.6	3
Super G (Microtherm)[d]	≈60% SiO_2 ≈37% TiO_2	300	90	0.1 (Pores)

[a] Frenzelit–Werke GmbH & Co. KG, P.O. Box 11 40, D-95456 Bad Berneck, Germany.
[b] Klevers GmbH & Co. KG, Oppelner Strasse 11, D-41199 Mönchenglad bach, Germany.
[c] ICI-Saffil Ltd., Pilkington Sullivan Site, Tanhouse Lane, Widnes, Cheshire, W A8 0RY, UK.
[d] Microtherm International Ltd., Industriepark Noord 1, B-9100 Sint Niklaas, Belgium.

were determined from preliminary measurements as $\varepsilon = 0.6$ for stainless steel and $\varepsilon = 0.05$ for gold, respectively [12]. Experimental data on samples without screens such as given in this figure, together with the definition of the effective thermal conductivity, Eq. (1), can be used to determine the mean extinction coefficient β.

In general, it is noted that the effect of radiation screens is to decrease the effective thermal conductivity with a decrease in the screen emissivity. The effect of the radiation screens can also be observed in decreased slopes of the conductivity curves. This is due to a significant reduction of radiative heat transfer in these layered systems, or, in other terms, an increased effective extinction coefficient. Additional results using different spacer materials are given elsewhere [12] and demonstrate conclusively the effect of screen emissivity on the effective thermal conductivity. For the sake of brevity, a part of these data are given together with theoretical results in the following section.

In Fig. 6 the influence of the screen is expressed by means of the dimensionless "gray pseudo extinction coefficient", β^*, which is the ratio of the extinction coefficient of the sample without screens to the extinction coefficient of the sample with screens. Therefore, β^* $(= \beta/\beta_s)$ describes the reduction of the radiation contribution to the total heat transfer rate. Symbols show the experimental data together with an approximation curve. As can easily be seen, β^* shows a dramatic decrease at lower emissivities, whereas little influence is evident for high screen emissivities.

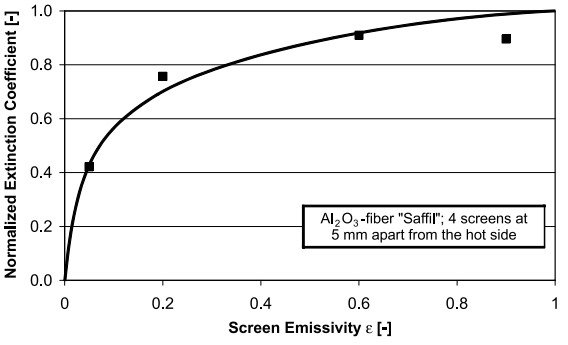

Fig. 6. Effect of screen emissivity on the normalized gray extinction coefficient: 30 mm ceramic fiber "Saffil" spacer material at $T_R = 700$ °C.

It should be noted that optimization leads to improvement of MTI for low screen emissivity whereas the screen influence increases with decreasing opacity of the spacer materials. This becomes evident when the dimensionless pseudo extinction coefficient β^* of fiber based MTI ($\beta = 5000\,\mathrm{m}^{-1}$, $\beta^*_{Au} = 0.4$) is compared with β^* of MTI based on microporous materials ($\beta = 30,000\,\mathrm{m}^{-1}$, $\beta^*_{Au} = 0.6$) while using gold screens.

4.2. Comparison of theoretical and experimental results

Results for three fiber spacers and microporous filler materials are available [12]. As the thermal performance of the three fiber spacer materials (Isotherm 1000, HT 1000 and Saffil) was very similar, results are given only for Saffil for the sake of brevity. The extinction coefficients used in the theoretical calculations are summarized in Table 2.

Figs. 7 and 8 show comparisons between predicted and measured effective thermal conductivities vs. T_R^3 for ceramic (Saffil) and microporous fillers, respectively. The dashed curves represent experimental values, whereas the solid curves denote the theoretical predictions. The extinction coefficient was determined by measuring k_{eff} of samples without screens and using Eq. (1), whereas the single scattering albedo was determined empirically. Therefore, albedoes were varied until the reduced conductivities which were experimentally measured with gold screens, could be confirmed analytically. Both the extinction coefficient and the albedo are given in the captions of the figures. The MTIs were 30 mm thick and had four equally spaced screens 5 mm apart starting from the hot side.

As can be seen in the Fig. 7, theoretical and experimental values yield a good correspondence with deviations below 10%. Note that extremely high scattering albedos ω near unity are needed for modeling a significant screen influence. This is due to a forward scattering

Table 2
Summary of effective extinction coefficient (β) and normalized extinction coefficient (β^*) for the MTIs constructed with four screens and different spacer materials

Material (manufacturer)	Extinction coefficient (1/m)	Effective extinction coefficient (1/m) (normalized extinction coefficient, β^*)			
		Black	SS steel	Ceramik	Gold
Isotherm 1000 (Frenzelit)	3812	–	4765 (1.25)	–	9073 (2.38)
HT 1000 (Klevers)	4844	–	4796 (0.99)	–	10,172[a] (2.10)
Saffil (ICI)	5097	5708 (1.12)	5607 (1.10)	6728[a] (1.32)	12,080[a] (2.37)
Super G (Microtherm)	17,900	–	45,182 (1.41)	–	40,055 (1.25)

[a] At a radiation temperature of 700 °C.

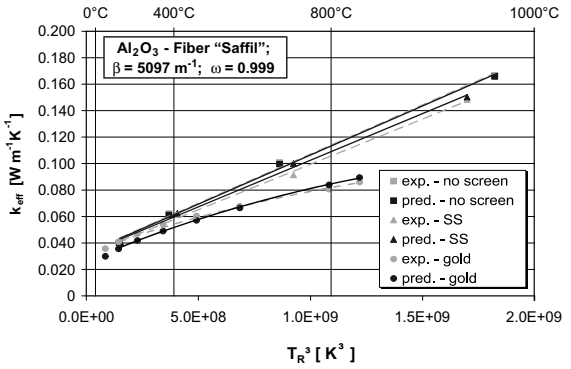

Fig. 7. Comparison of measured and predicted effective thermal conductivities for 30 mm ceramic fiber ("Saffil"), four screens, $\beta = 5097$ m^{-1} and $\omega = 0.999$. Dashed curves show experimental values and solid curves theoretical predictions.

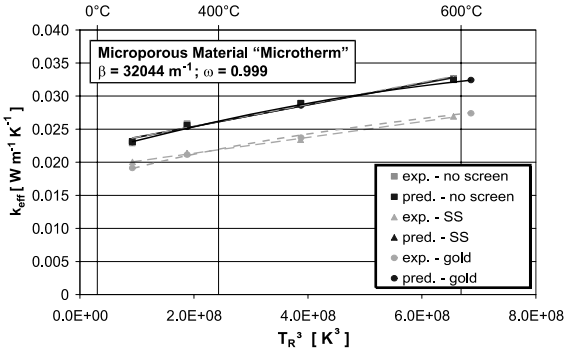

Fig. 8. Comparison of measured and predicted effective thermal conductivities for 30 mm microporous material ("Microtherm Super G"), four screens, $\beta = 32,044$ m^{-1} and $\omega = 0.999$. Dashed curves show experimental values and solid curves theoretical predictions.

tendency in the fiber materials under investigation. Fig. 8 is showing totally different results. The model does not correctly predict the influence of the screens. It must be said that this discrepancy between model predictions and the experimental data is believed to be due to the model limitations discussed above. Highly absorbing infrared opacifiers have been added to the microporous spacer materials at a mass percentage of 30%.

4.3. Optimization of MTI

The theoretical model developed was used to optimize the design of the MTI. The model parameters include the number of screens and their locations, spacer material, thickness of spacer material, total thickness of the insulation as well as the highest temperature of the insulation surface. Some sample results of calculations

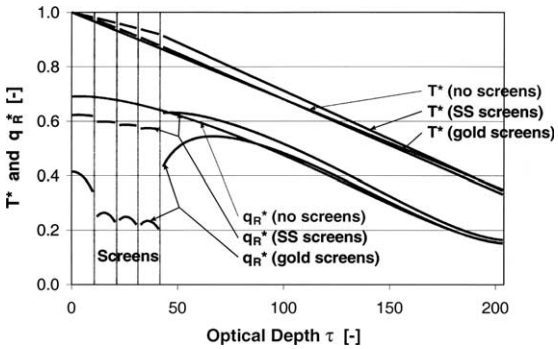

Fig. 9. Effect of screens on the dimensionless temperature and radiant heat flux fraction profiles vs. the optical depth: Al_2O_3-fiber filler, $T_1 = 1000$ °C, $q = 1900$ W/m^2, four SS alloy and gold screens placed as shown.

are illustrated and discussed below for ceramic fiber and microporous filler materials.

The dimensionless temperatures and fractional radiant heat flux profiles for Al_2O_3-fiber filler material are shown in Fig. 9 as a function of the optical thickness of the layer (excluding the very thin screens). The entire sample thickness is now 40 mm or $\tau = 204$, respectively, with four equally spaced screens 2 mm apart starting at the hot side. Results are reported for an insulation with and without four alloy and gold screens. The locations of the screens are indicated in the figure. Note that the temperature profile is continuous, but the dimensionless radiation heat flux varies in a discontinuous manner at the screen surfaces. The continuity of the total heat flux is insured as required by the conservation of energy equation, Eq. (1). Also as expected, the discontinuities of the q_R^* are greater for gold than for stainless steel screens, because the former has a much lower emissivity (higher reflectivity). It should be mentioned that the enhanced radiative heat flux in the vicinity of the cold side of the last screen is due to the emitted flux of the screen itself, which is interfering a constant radiative flux profile. This affects also the temperature profiles in the vicinity of the screens, whereas the cold side temperature is as expected.

Similar results for dimensionless temperature and fractional radiant heat flux vs. optical thickness are illustrated in Fig. 10 for a microporous material. Again, sample thickness is 40 mm or $\tau = 1282$, respectively, with four equally spaced screens 2 mm apart starting at the hot side. Comparison of Figs. 9 and 10 shows that radiation accounts for a larger fraction of the total heat flux through the $A1_2O_3$-fiber MTI than the microporous material filler MTI. At the cold face of the MTI more than about 95% of total heat transfer rate is by conduction in the microporous material and only about 85% in the silicon fiber filler material. The total heat flux through the $A1_2O_3$-fiber filler material MTI without the

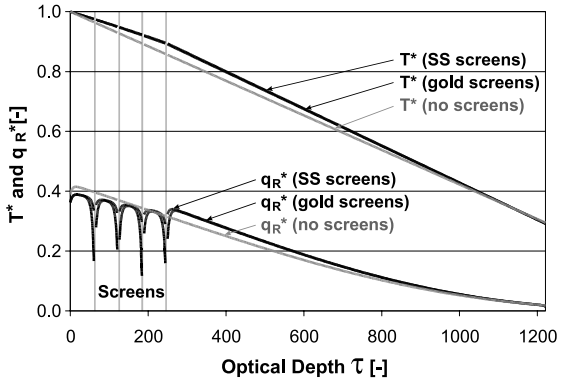

Fig. 10. Effect of screens on the dimensionless temperature and radiant heat flux fraction profiles vs. the optical depth: microporous material filler, $T_1 = 1000$ °C, $q = 760$ W/m^2, four SS alloy and gold screens placed as shown.

screens is 1900 W/m^2 while the total heat flux through the microporous filler material is 760 W/m^2. This clearly indicates that the microporous material (Microtherm Super G) is thermally more effective than the silicon fiber material (Saffil).

5. Concluding remarks

The problem studied involved the development of high temperature multilayer thermal insulations for an application to MCFC and SOFC fuel cell power plants. Therefore, both experimental and theoretical studies were carried out in parallel.

The experimental investigations led to a new design of guarded hot plate apparatus. Calorimetric measurements were made with the apparatus, and the influence of radiation screens on the effective thermal conductivity of layered insulation systems was investigated systematically. The lowest thermal conductivity MTI were achieved with microporous materials.

Radiation screens generally reduce more or less the effective thermal conductivity of the stand-alone spacer. A combination of low emissivity screens and optically thin spacers yield optimal reduction of the effective thermal conductivity, whereas additional screens show only limited influence.

For numerical simulation of the combined conduction and radiation heat transfer in porous layered media the energy conservation equation approach was used together with a scaling model reported by Lee and Buckius [13] for predicting heat transfer in porous materials with screens. The model predictions agree with experimental results for fibrous spacer materials. The assumption of gray radiation properties, therefore, seems to be appropriate. Limitations of the model appear evident for microporous spacer materials to which highly absorbing opacifiers have been added.

References

[1] M. Jakob, G.A. Hawkins, Elements of Heat Transfer and Insulations, second ed., Wiley, New York, 1950.
[2] J.F. Malloy, Thermal Insulation, Van Nostrand-Reinhold, Princeton, NJ, 1959.
[3] C.L. Tien, G.R. Cunnington, Cryogenic insulation heat transfer, in: T.F. Irvine Jr., J.P. Hartnett (Eds.), Advances in Heat Transfer, Vol. 9, Academic Press, New York, 1973, pp. 349–417.
[4] R.L. Dotts, H.H. Battley, J.T. Hughes, W.E. Neuenschwander, Shuttle orbiter reusable surface insulation thermal performance, in: AIAA 20th Aerospace Sciences Meeting, Orlando, FL, Paper AIAA-82-0005.
[5] M. Giegerich, K. Handrick, Flight test verification of current generation ceramic- based TPS, in: Proceedings of the 3rd European Workshop on Thermal Protection Systems, ESTEC, Noordwijk (NL), 1998.
[6] L.J.M.J. Blomen, M.N. Mugerwa (Eds.), Fuel Cell Systems, Plenum Press, New York, 1993.
[7] J.H. Hirschenfelder, Fuel cell status, in: Proceedings of the Intersociety Energy Engineering Conference, IEEE, New York, 1996, pp. 1084–1089.
[8] M. Kaviany, B.P. Singh, Radiative heat transfer in porous media, in: J.P. Hartnett, T.F. Irvine Jr., Y.I. Cho (Eds.), Advances in Heat Transfer, Vol. 3, Academic Press, Boston, 1993, pp. 133–186.
[9] K. Kamiuto, S.S. Yee, Elementary transport processes in packed beds of spheres, in: Trends in Heat, Mass and Momentum Transfer, Vol. 7, Research Trends, Trivandrum, India, 2001, pp. 349–417.
[10] C. Stark, J. Fricke, Improved heat-transfer models for fibrous insulations, Int. J. Heat Mass Transfer 36 (1993) 617–625.
[11] H. Reiss, Radiative Transfer in Nontransparent Dispersed Media, Springer-Verlag, Berlin, 1988.
[12] M. Spinnler, Experimentelle und Theoretische Untersuchungen an Warmedammsystemen für Hochtemperatur-Brennstoffzellen, Dissertation, Technische Universität München, Garching, 2001.
[13] H. Kuchling, Taschenbuch der Physik, Verlag Harry Deutsch, Frankfurt, 1989.
[14] H. Lee, R.O. Buckius, Combined mode heat transfer analysis utilizing radiation scaling, High Temp.–High Pressures 17 (1985) 167–274.
[15] R. Viskanta, Heat transfer by conduction and radiation in absorbing and scattering materials, ASME J. Heat Transfer 87 (1965) 143–150.
[16] W.W. Yuen, L.W. Wong, Heat transfer by conduction and radiation in a one-dimensional absorbing, emitting and anisotropically scattering medium, ASME J. Heat Transfer 102 (1980) 303–307.
[17] Verein Deutscher Ingenieure, DIN 52 616—Bestimmung der Warmeleitfahigkeit mit dem Warmestrommel3platten-Gerat, in: Deutsche Normen, Beuth Verlag, Berlin, 1977.